Energy absorption capacity of agglomerated cork under severe loading conditions

Influence of temperature and strain rate

Louise Le Barbenchon · Philippe Viot · Jeremie Girardot · Jean-Benoit Kopp

Abstract Understanding the mechanical behavior of materials in working conditions is a current problem in transport industries. In this article, we demonstrate why the temperature and the strain-rate are first-order parameters when studying the mechanical behavior of polymeric cellular materials with a glass transition temperature T_g in working temperatures. Compressive tests in quasi-static until a 0.5 hencky strain were conducted at several temperatures on agglomerated cork. Compressive tests were then conduted along a large range of strain rates, from 4.2 10^{-5} s^{-1} to 250 s^{-1} at room temperature (24°C). Both parameters influence strongly the overall mechanical behavior with an opposite effect because of the polymeric nature of the constitutive materials. However discrepencies in the variation were observed between materials parameters of the two conditions (temperature and strain rate).

In order to separate the dynamic effects from the modification of the stiffness of the constitutive materials with temperature or strain rate, a specific apparatus was designed to achieve high-strain rate tests in temperature. Compressive tests in dynamic regime were then conducted at -20°C on agglomerated cork as a proof-of-concept. The experimental results (stress/strain curves and materials parameters) showed a great influence of the strain-rate and the temperature combined. Such apparatus will provide results allowing a more in-depth characterisation of the local mechanisms that will be precious for future simulations.

Louise Le Barbenchon
Arts et Metiers Institute of Technology
CNRS, I2M Bordeaux, Esplanade des Arts et Metiers,
F-33405 Talence Cedex, France
E-mail: louise.le_barbenchon@ensam.eu

Keywords Polymeric foam · Cellular Material · Microstructure · Cork Agglomerate · Temperature · Non-linear Mechanical Behavior · Dynamic loadings · Energy absorption

1 Introduction

The demand for lighter and bio-sourced materials is currently increasing because of emerging concerns about global warming. Cork presents a unique set of properties (fire resistant, impact absorbing, phonic isolation ...) due to its foam structure and polymeric composition [1]. It is therefore an excellent candidate for a wide range of application domains. One of them is aeronautical parts with an usual temperature range around [-30°C, 80°C] and loading conditions that can vary from an impact due to a tool drop to the protection of the structure from fragment impact in the space.

Due to the polymeric nature of cork, temperature highly influences the mechanical behavior of cork and its co-products like agglomerated cork [2–4]. Cork agglomerates have a mechanical behavior which decreases when temperature is rising. However, no link was clearly demonstrated between the polymeric nature of the material and the non-linear mechanical behavior at several temperatures for cork-based cellular materials.

As cork agglomerates are used in energy absorption, their mechanical behavior under dynamic strain rates has been studied, principally by testing cork structures through impact tests achieved with a drop tower [5–8]. An increase in macroscopic stresses was usually noted with the increase in the initial strain-rate [7]. However, the type of set-up did not allow to reach a constant loading rate during a compression test and no material parameter could be deduced from it. These parameters

are however essential in order to simulate the mechanical behavior under complex sollicitations [5].

Hopkinson bars were often used to test cork-based materials at high strain rates. Recent works use Digital Image Correlation (DIC) in order to evaluate the actual strain distribution at a cork agglomerate sample surface tested during Hopkinson bars tests [9]. 2D DIC results show a significant strain heterogeneity within each sample surface. However, these tests in dynamic regimes did not allow to reach important strains [9] and raw signals presented a lot of noise [10]. The strain-rate varied also during the compression loading [11] which induces error in the material parameter identification.

Moreover, the mechanical behavior of cork agglomerates was evaluated under several temperatures during impact loadings to simulate working environmental conditions [12]. No important changes were noted between 21°C and 50°C. However, in another study when cork agglomerates are impacted between -30°C and 100°C, an important decrease in the absorbed energy during an impact with an increase of the temperature is observed especially for high-energy impacts [13]. Furthermore, it seems that the influence of the temperature on the absorbed energy rises with the specimen density [13]. Such results demonstrate the necessity of studying the mechanical behavior of materials under temperature and strain rate working conditions. However, as they are performed at the industrial part scale, they do not allow to understand the underlying micromechanisms (at the scale of the cell or the bead) that cause such dependencies in the mechanical behavior.

Concerning agglomerated cork, it seems there is a lack of material characterisation of the non-linear mechanical behavior under both large ranges of strain-rate and temperature. Fine material characterisation is required in order to model its mechanical response. The aim of this work is to study the mechanical behavior of cork agglomerates under large strains and its dependency to the strain-rate and the temperature to see how it affects the energy absorption capacities of cork agglomerates.

Compression tests were conducted at several temperatures and at different strain rates. To reproduce working conditions, a thermal chamber was specially designed to perform compression tests in dynamic regime at high and low temperatures with a constant strain rate. Several type of samples were tested to be able to draw general conclusions from this experimental series of tests.

2 Material & Methods

2.1 Materials

Agglomerated cork are obtained by mixing small beads ($\oslash \approx [0.5, 1]$ mm) together with a bio-sourced thermosetting resin (polyfurfuryl alcohol, PFA). Two types of agglomerated cork were studied: one with short fibres (R for *reinforced* with fiber dimensions: $\oslash \approx 7$ μm, l $\approx$ 170 μm) and one without fibres (NR for *non-reinforced*) [14]. For the reinforced one, fibres were added at this step of the process. The mixture is then compressed into a mold to obtain a $1000 \times 500 \times 150$ mm^3 block. During the molding, the compression induces a preferential orientation of the beads in the (Oxy) plane [15].

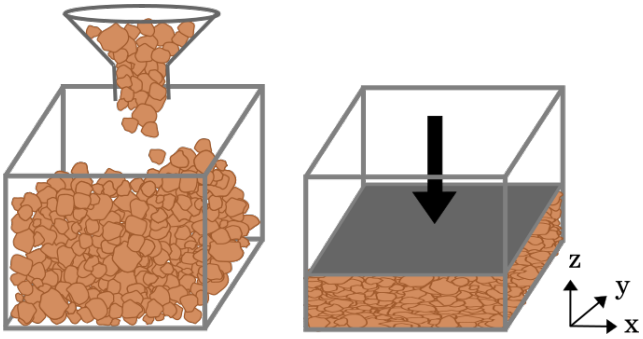

(a) Compression step during the manufacturing process.

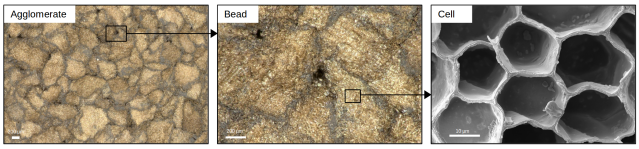

(b) Resulting multi-scale structure.

Fig. 1 (a) Manufacturing process. Cork beads coated with resin are poured inside a metallic mold then compressed uniaxially in the (Oz) direction. (b) Pictures of the resulting agglomerate cork at several observation scales.

Two directions induced by the bead flattening are considered (Fig. 1(a)): directions in the (Oxy) plane will be called in-plane directions (IP) and (Oz) direction will be called out-of-plane direction (OP). The polymerisation was made in an autoclave at 130°C during 12 hours. Large plates were then machined from the block.

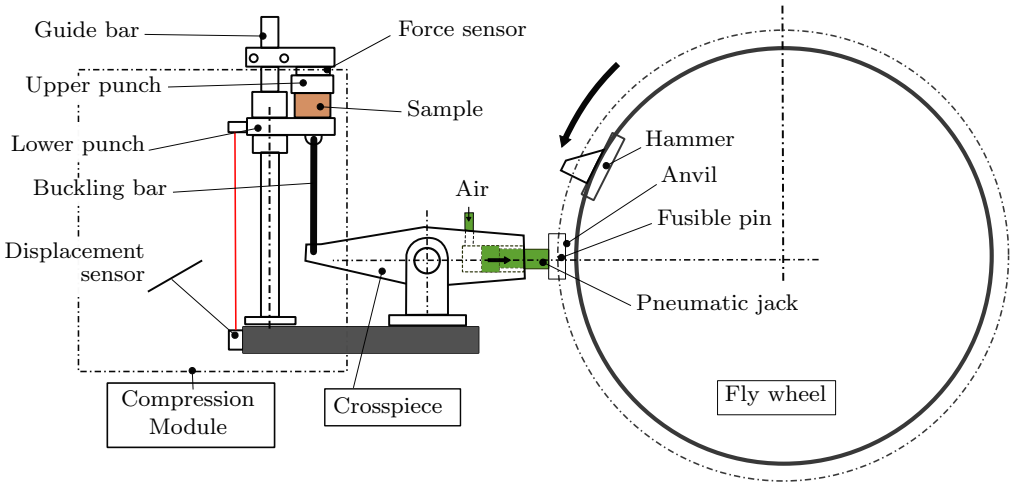

Fig. 2 Scheme of the flywheel and the compression device [16].

2.2 Quasi-static regime

2.2.1 Tests at room temperature

$20 \times 20 \times 20\ mm^3$ samples were cut. Their density was measured and stands around 420 $kg\ m^{-3}$ as the cork behavior depends on this parameter [7]. Samples were conditioned at a 50% relative humidity to reduce the potential effect of hygrometry [4].

An electromechanical tensile/compression machine (Zwick Roell 250) with a load cell capacity of 250 kN was used. The imposed speed of the lower punch was set at 0.05, 5, 500 $mm\ min^{-1}$ corresponding to average strain rates of 4.2 $10^{-5}\ s^{-1}$, 4.2 $10^{-3}\ s^{-1}$ and 4.2 $10^{-1}\ s^{-1}$. The mechanical behavior of the two main directions, in-plane (IP) and out-of-plane (OP), was investigated. Five specimens of each material were tested for both directions at each strain-rate.

2.2.2 Compression at different temperatures

At 4.2 $10^{-3}\ s^{-1}$, four temperature conditions were set: -30°C, -10°C, 80°C and the room temperature measured at 24°C. The temperature was controled in a chamber (Zwick) equipped with a heater (for the 80°C temperature) and a nitrogen cooling connector (for the temperatures of -30°C and -10°C) with an induced circulation to keep the temperature constant in the chamber during the tests. Samples were placed at least one hour beforehand in the chamber at the wanted temperature in order to reach a stabilised temperature. The temperature was checked using infrared temperature sensor. Five specimens of each agglomerate were tested for all temperatures in both directions.

2.3 Intermediate dynamic compression regime

To reach higher levels of strain rates, cork samples were tested on a flywheel. It is an original apparatus which allows to dynamically load specimens at intermediate strain rates (from 50 to 800 s^{-1}) [17].

A test on the flywheel can be described as follows (Fig. 2): the heavy metallic wheel (1 m diameter, 617 kg) is set in motion and its rotation velocity is accurately controlled by an asynchronous motor. A hammer fixed on the wheel is the impactor of this machine and can impose either tensile loadings on metallic and composite materials or compressive loadings on cellular materials according the complementary apparatus being used [18].

To carry out compression tests on cork material, when the desired rotation speed of the wheel is reached, a pneumatic jack pushes the anvil alongside the wheel. The anvil is then grabbed by the hammer inducing a rapid rotation of the crosspiece. This rotation imposes the displacement of the buckling bar and the lower punch. Once the compressive force reaches a predetermined threshold value, the bar buckles and interrupts further specimen compression. The unloading however is not controlled and is not operated at the same strain rate.

This device, due to its high moment of inertia (77 $kg\ m^2$), enables the compression of specimens under constant velocity, since the specimen does not absorb enough energy to slow the wheel down.

The compressive stress is measured by a piezo-electric KISTLER 9031A force sensor located behind the upper punch and coupled with a charge amplifier KISLTER 5018A1000. The lower punch displacement is determined by a dynamic laser sensor Micro-epsilon LD1627-27. Raw signals were used as they presented low noises.

At least four samples were tested for each test configuration (material, direction, strain-rate). A high speed camera Photron SA5 and appropriate lighting were placed in front of the compression module to be able to observe samples during loading. The image frequency was set at 9300 frame per second.

2.4 Experimental compression curves post-treatment

From the force $F(t)$ and the displacement $d(t)$ data, macroscopic stress/strain curves were deducted by calculating nominal stress ($\sigma = \frac{F(t)}{S_0}$) and true strain ($\varepsilon = ln(\frac{l_0 - d(t)}{l_0})$), l_0 being the initial height of the sample and S_0, the initial surface of the sample.

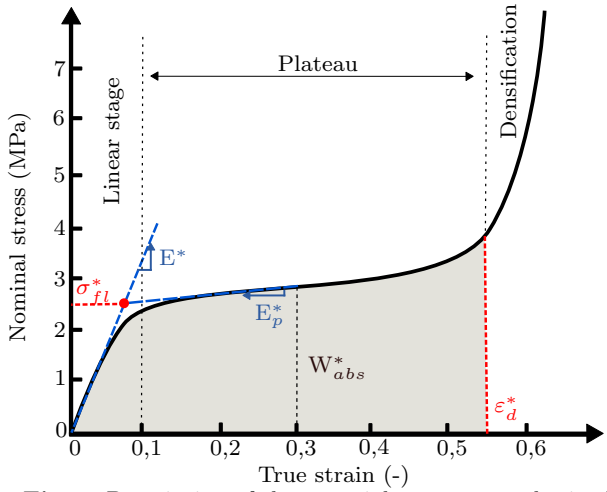

Fig. 3 Description of the material parameters obtained from the stress/strain exprimental curve.

The Young's modulus E^* is calculated between a low strain ε_0, arbitrary fixed to 0.001, and 80% of the strain ε_r (strain at the transition between linear and plateau response). To determine the transition strain ε_r, the curve was fitted with a polynomial function. The inflection point of the elastic part of the curve was found with its second derivative. The Young's modulus is then calculated from the mean slope of the experimental curve between the two strains ε_0 and $0.8\varepsilon_r$.

The plateau modulus E_p^* is measured between a true strain of 0.1 and 0.3 from the mean slope of the experimental curve (Fig. 3). The macroscopic buckling stress σ_{fl}^* is identified as the stress at which the line with a slope of E^* and the line with a slope of E_p^* cross (Fig. 3).

An energy efficiency parameter η is defined as,

$$\eta(\varepsilon) = \frac{1}{\sigma(\varepsilon)} \int_0^{\varepsilon} \sigma(\varepsilon) d\varepsilon. \tag{1}$$

The onset of the densification ε_{d^*} can be identified as the strain at which η reaches a maximum on the efficiency-strain curve [19,20],

$$\frac{d\eta(\varepsilon)}{d\varepsilon}_{\varepsilon=\varepsilon_{d^*}} = 0. \tag{2}$$

The energy absorbed until the initiation of the densification W_{abs}^* corresponds to the sum of dissipated and elastic energies until the end of the plateau (Fig. 3).

$$W_{abs}^* = \int_0^{\varepsilon=\varepsilon_d^*} \sigma(\varepsilon) d\varepsilon \tag{3}$$

It is obtained by integrating along the strain using the composite trapezoidal rule until ε_{d^*} (eq. 3). To be able to compare it with literature data, the energy calculated was divided by the sample volume.

For each set of data, the standard deviation σ_{SD} was calculated, with N, the number of samples tested and $\overline{x}$, the mean value of the data set,

$$\sigma_{SD} = \sqrt{\frac{1}{N-1} \sum_{i=1}^{N} (x_i - \overline{x})^2}. \tag{4}$$

3 Results & Discussion

3.1 Effect of temperature

3.1.1 Macroscopic response

Fig.4 shows the experimental stress/strain curves of cork agglomerates tested in quasi-static (5 mm/min) uni-axial compression at several temperatures (from -30°C to around 100°C). Both directions (IP and OP) and both types of agglomerates (R and NR) are visible. For each temperature, cork agglomerates show a typical cellular mechanical behavior with the three stages: linear, plateau and densification. Reinforced (R) and non-reinforced (NR) cork agglomerates loaded in the IP direction show higher stresses for the same temperature. This is mainly due to the structure at the bead scale as already reported for high density agglomerates [15].

As already observed in the case of many polymeric materials, a higher stress is required to achieve the same macroscopic strain as temperature is decreasing [21,22].

The temperature dependency of the mechanical behavior of cork agglomerates is not surprising. Indeed, the whole material is a composite made of several polymeric materials. On one hand, the stiffness of the thermosetting resin is expected to have a relatively linear

Material	ε^*_{frac} at -30°C	ε^*_{frac} at -10°C	ε^*_{frac} at 24°C	ε^*_{frac} at 80°C
R-OP	X	X	X	X
NR-OP	$0.42^{\pm 0.03}$	$0{,}45^{\pm 0.01}$	X	X
R-IP	$0.38^{\pm 0.02}$	$0.45^{\pm 0.01}$	X	X
NR-IP	$0.33^{\pm 0.03}$	$0.35^{\pm 0.02}$	$0.43^{\pm 0.05}$	$0.47^{\pm 0.04}$

Table 1 Macroscopic strain ε^*_{frac} at which cracks are observed at the sample surface during an uni-axial compression loading at 4,2 10^{-3} s^{-1} at several temperatures. X : no crack is noticed during or after the test.

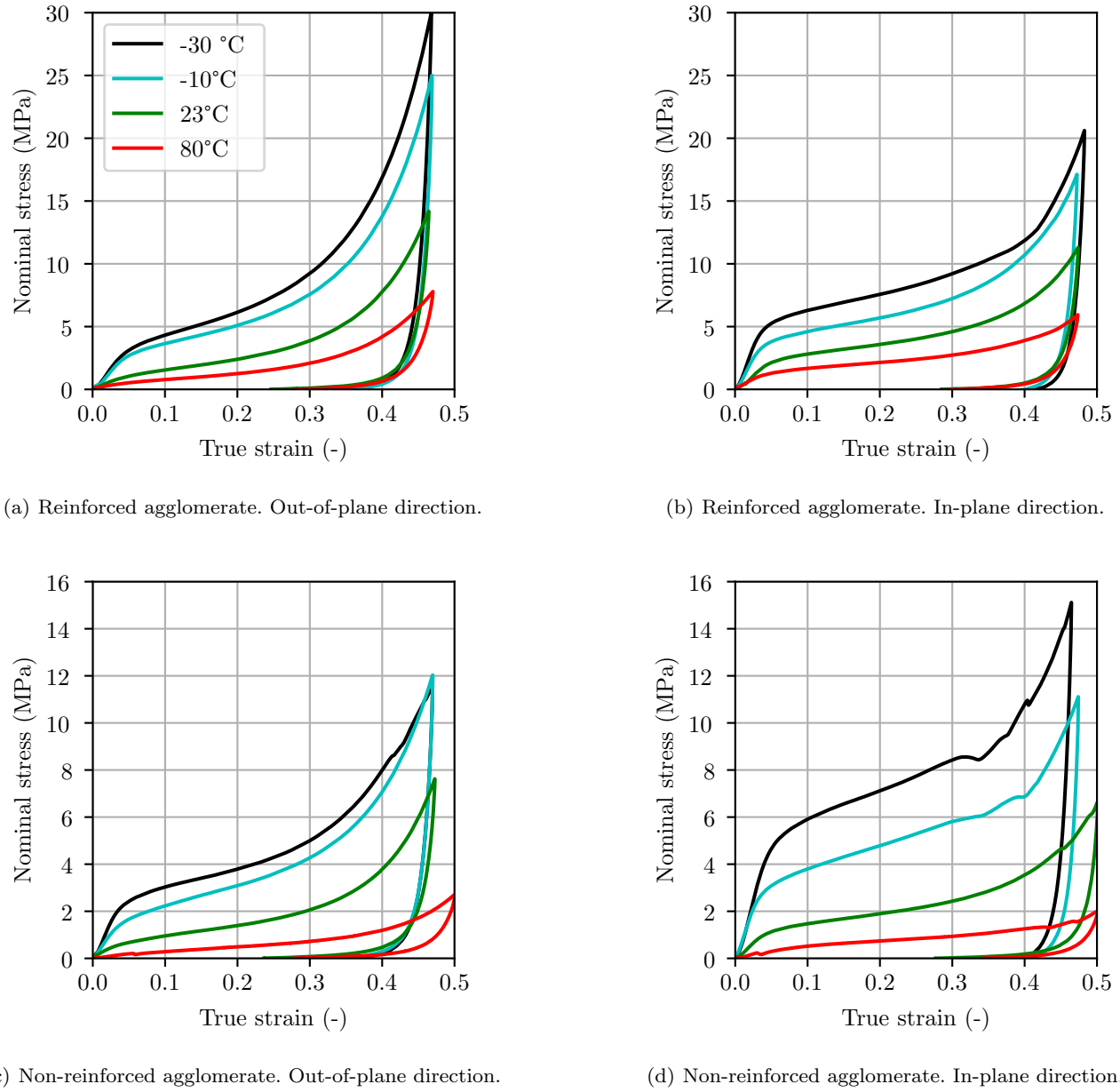

(a) Reinforced agglomerate. Out-of-plane direction.

(b) Reinforced agglomerate. In-plane direction.

(c) Non-reinforced agglomerate. Out-of-plane direction.

(d) Non-reinforced agglomerate. In-plane direction.

Fig. 4 Experimental stress/strain curves of cork agglomerates samples loaded in compression at a mean strain rate of 4.2 10^{-3} s^{-1} in the in-plane (IP) and out-of-plane (OP) direction at several temperatures.

dependency to the temperature on a over a broad temperature range (the glass transition temperature T_g being high). On the other hand, cork cells walls are made of several thermoplastic polymeric substances that have a temperature dependent mechanical behavior [23,24]. It seems thus natural that the mechanical behavior of

agglomerated cork is also strongly temperature dependent.

3.1.2 Fracture mechanisms

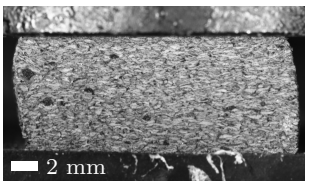

(a) Reinforced - Out-of-plane

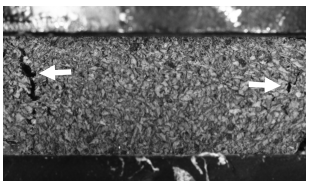

(b) Reinforced - In-plane

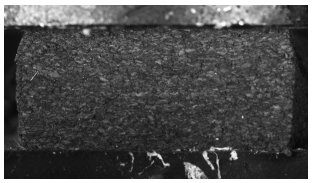

(c) Out-of-plane

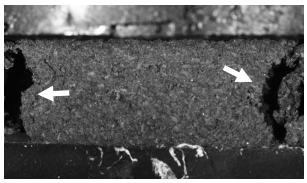

(d) In-plane

Fig. 5 Pictures of sample surface at the maximal imposed strain during a quasi-static compressive loading at -30°C.

The macroscopic strain ε^*_{frac} at which fracture is observed at the sample surface has been reported in tab. 1. For all agglomerates, lower temperatures lead to earlier macroscopic failure as ε^*_{frac} decreases with temperature. In agglomerated cork, fracture mechanisms are mostly intra-granular [14]. This decrease in the fracture strain with temperature would thus be mainly due to the tensile embrittlement of the cork beads and thus the cork cell walls with the drop in temperature. It has already been shown that carbon fibres in cork agglomerates could prevent initiation of a macroscopic crack due to the confinement of micro-cracks [14]. This tendency is therefore also valid for a large temperature range.

The non-reinforced cork agglomerate compressed in the in-plane direction (IP) is the most sensitive to fracture mechanisms at room temperature as previously mentionned in [14]. Fracture mechanisms occur earlier with decreasing temperature as evidenced by stress slope failures during compression (Fig. 4(d)). They appear at $\varepsilon^*_{frac} = 0.47 \pm 0.04$ at 80°C while they are observed from $\varepsilon^*_{frac} = 0.33 \pm 0.03$ at -30°C (tab. 1).

At low temperatures, cracks are also observed in non-reinforced agglomerated cork compressed in the out-of-plane direction (NR-OP) and reinforced agglomerated cork loaded in the in-plane direction (R-IP) (tab. 1).

These fracture mechanisms are problematic for the identification of the material parameters. Indeed, once macroscopic cracks are present inside the sample, hypothesis of continuity cannot be made anymore. It is then important to note the strain ε^*_{frac} at which surface hypothesis and thus material parameters are not valid anymore. For non-reinforced agglomerates, fracture mechanisms are visible from -10°C, at $\varepsilon^*_{frac} = 0.45 \pm 0.01$ on the stress/strain curve (Fig. 4(c)). This information is thus easily available. However, concerning reinforced agglomerates, the macroscopic curve is not sufficient to be able to tell when fracture is happening. While the macroscopic stress/strain curve (Fig. 4(b)) does not show any sudden change of slope, macroscopic cracks can be spotted at the sample surface (Fig. 5).

3.1.3 Evolution of the material parameters with temperature

The variation of the material parameters as a function of the temperature of the cork agglomerates tested was obtained from the macroscopic curves (Fig. 6). The error bars are obtained from the calculation of the standard deviation σ_{SD}.

As the temperature increases, the Young's modulus E^* decreases non-linearly for all the cork agglomerates (Fig. 6(a)). The decrease in Young's modulus E^* is significant between -30°C and 25°C. It is thus less important for temperatures above 25°C. Except for the strain at the initiation of the densification ε^*_d, material parameters such as buckling stress σ^*_{fl} (Fig. 6(b)) and tangent modulus E^*_p (Fig. 6(c)) evolve in the relatively same way with temperature (Fig. 6).

This temperature dependency is highly correlated to the temperature dependency of the storage modulus E' of cork obtained by vibratory tests [4]. The glass transition temperature T_g of the agglomerates samples is around 20.2°C and 40.3°C for the non-reinforced and the reinforced agglomerate, respectively [14]. It is around these temperatures that the variation of the mechanical behavior of agglomerated cork with the temperature starts to decrease (Fig. 6(a) and Fig.6(b)).

This kind of vibratory test allows to study the visco-elastic behavior of polymeric materials, *i.e.* for very small strains. For other cork-based materials, it has been shown that the visco-elastic behavior comes from the temperature dependency of cork cell walls [25]. The resin can add a supplementary relaxation like agglomerated cork with poly-urethane [25] or polyfurfuryl alcohol [26,14] but only for high temperatures. Therefore, the thermoset resin does not play an important role in the temperature dependency in this temperature range. The variations of the material parameters with temperature reflect the variations of the cork cell walls behavior.

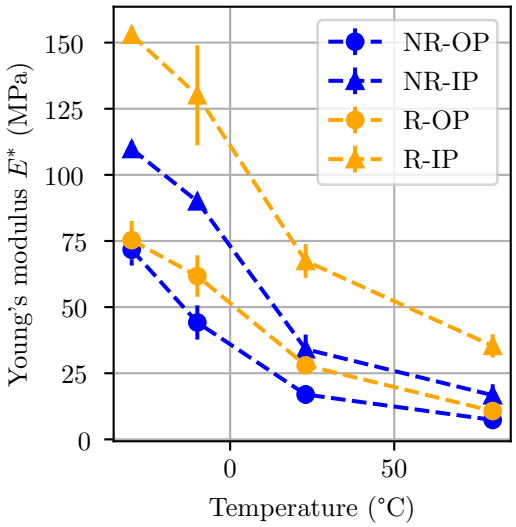

(a) Young's modulus.

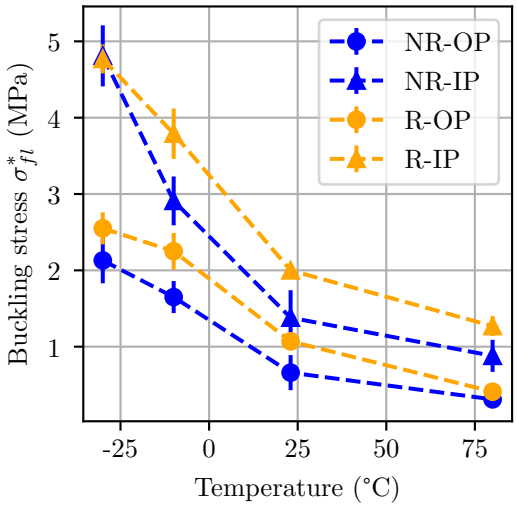

(b) Buckling stress.

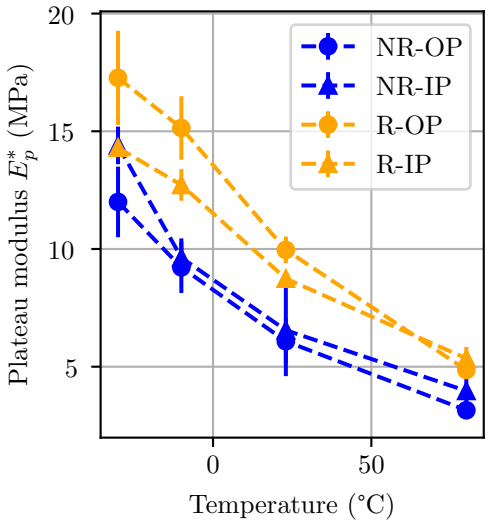

(c) Plateau modulus.

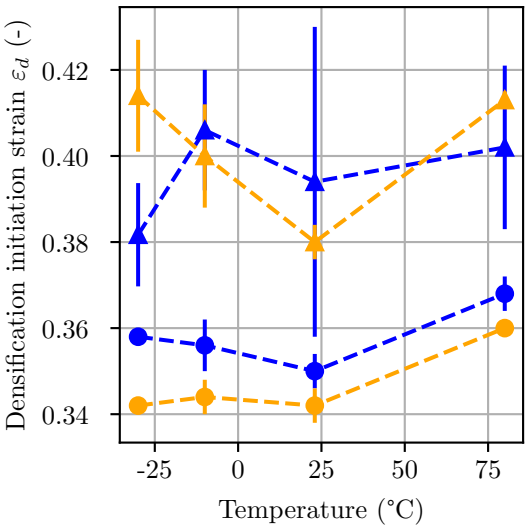

(d) Densification strain.

Fig. 6 Material parameters of different cork agglomerates compressed at a mean strain rate of 4.2 10^{-3} s^{-1} at several temperatures.

According to the Gibson and Ashby model [27] on the mechanical behavior of cellular materials,

$$\sigma^*_{fl} \simeq \frac{\pi^2 E_s I}{l^2}, \tag{5}$$

with E_s the Young's modulus of the cell wall material, I, the quadratic inertia and l, the cell wall length. Therefore, σ^*_{fl} should have the same variation as E_s with temperature. The variation of the storage modulus E' of cork reflects the local variation of E_s of cork cell walls and more macroscopically E^*. Therefore, σ^*_{fl} and E^* should have the same temperature dependency, which is what is observed experimentally (Fig. 6(a) and Fig. 6(b)).

The tangent modulus E^*_p varies more linearly with temperature (Fig. 6(c)). Many models are based solely on the influence of the gas [27,28] concerning the stress hardening in the plateau phase. They do not into account the influence of the microstructure or the evolution of the mechanical behavior of the constituent material (or by considering it as perfect elastoplastic), even though it is locally stressed at high stress levels [29]. Yet this temperature dependence is the proof that other

mechanisms are implicated during the plateau phase. More recent work shows that the non-zero slope of the plateau could depend on both on architectural effects and on the visco-plastic behavior of the wall material [30] in the case of metallic foams. According to 2D finite element modelling of a metallic open cell foam [31], the combination of architectural effects (stress localisation) and work hardening of the constituent material could be at the origin of this slope.

The fact that E_p^* decreases strongly with the temperature (Fig. 6(c)) shows here that it depends strongly on the cell wall behavior. But as this variation is slightly different from σ_{fl}^* and E^*, this means that supplementary effects have to be taken into account if one wish to go further in the description of the mechanisms implicated in the plateau phase.

For the Young's modulus E^*, the buckling stress σ_{fl}^* and the plateau modulus E_p^*, the standard deviation σ_{SD} is rather limited. This is mainly due to the strict control of the test conditions (loading, temperature, hygrometry). The size of the specimens is moreover well representative of the mechanical behavior of the agglomerates given the size of the beads and the cells [15].

Concerning the strain ε_d^* at the onset of the densification (Fig. 6(d)), it seems to be stable with the temperature as already observed for birch plywood [32]. The non-reinforced cork agglomerate loaded in the in-plane direction shows an important standard deviation for ε_d^* in comparison to the other samples (Fig. 6(d)). This could be due to the more fragile behavior of this specimen.

It can be concluded that the temperature dependency of the non-linear mechanical behavior of cork-based material is mainly due to the temperature dependency of the visco-elastic behavior of the constitutive materials of cork cell walls. Having a glass transition temperature T_g right in the range of use and near room temperature implies caution regarding the temperature when considering the mechanical behavior: linear and non-linear. If one of the constitutive material (here cork) has an elastic behavior with an highly viscous part, the non-linear mechanical behavior will be strongly modified with temperature apart from the strain at the onset of densification.

3.1.4 Absorbed energy variation with the temperature

Measuring the absorbed energy W_{abs}^* until the densification initation strain ε_d^* allows to quantify the mechanical energy absorption properties of a material before the stress strongly increases.

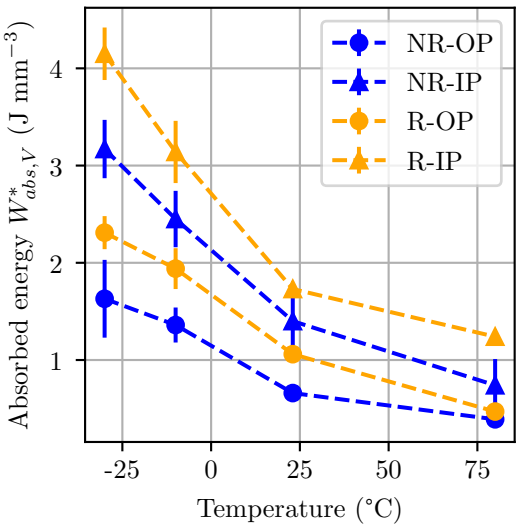

Fig. 7 Volumic absorbed energy at the initiation of the densification for different types of agglomerated cork under several temperature conditions.

Absorbed energy is the sum of the elastic and dissipated energy. The latter depends on the residual strain and fracture mechanisms. That is why, despite macroscopic cracks observed at the sample surface, this energy is calculated way beyond ε_{frac}^*.

The influence of temperature on the absorbed energy W_{abs}^* is quite the same as for E^*, σ_{fl}^* and E_p^* (Fig. 7). Before 25°C, it decreases quickly with the temperature approaching the glass transition temperature. For higher temperatures, W_{abs}^* is still decreasing but less rapidly. Mathematically, W_{abs}^* depends on all those parameters (eq.1). This is why they share the same temperature dependency.

The change of the temperature causes a variation in the mechanical energy absorption capacity for all tested materials. But the hierarchy between the most asborbant materials stays the same. At low and high temperature, the most absorbant material is the stiffest, with the highest plateau: the reinforced agglomerate loaded in the in-plane direction (R-IP) (Fig. 7).

3.2 Effect of the strain rate

Cork-based materials are expected to be strongly strain-rate dependent because of their polymeric constitution and their architectured microstructure. Besides cork agglomerate is considered for impact absorption. It is thus important to characterise its mechanical behavior at several strain rates and to understand the strain mechanisms at different scales.

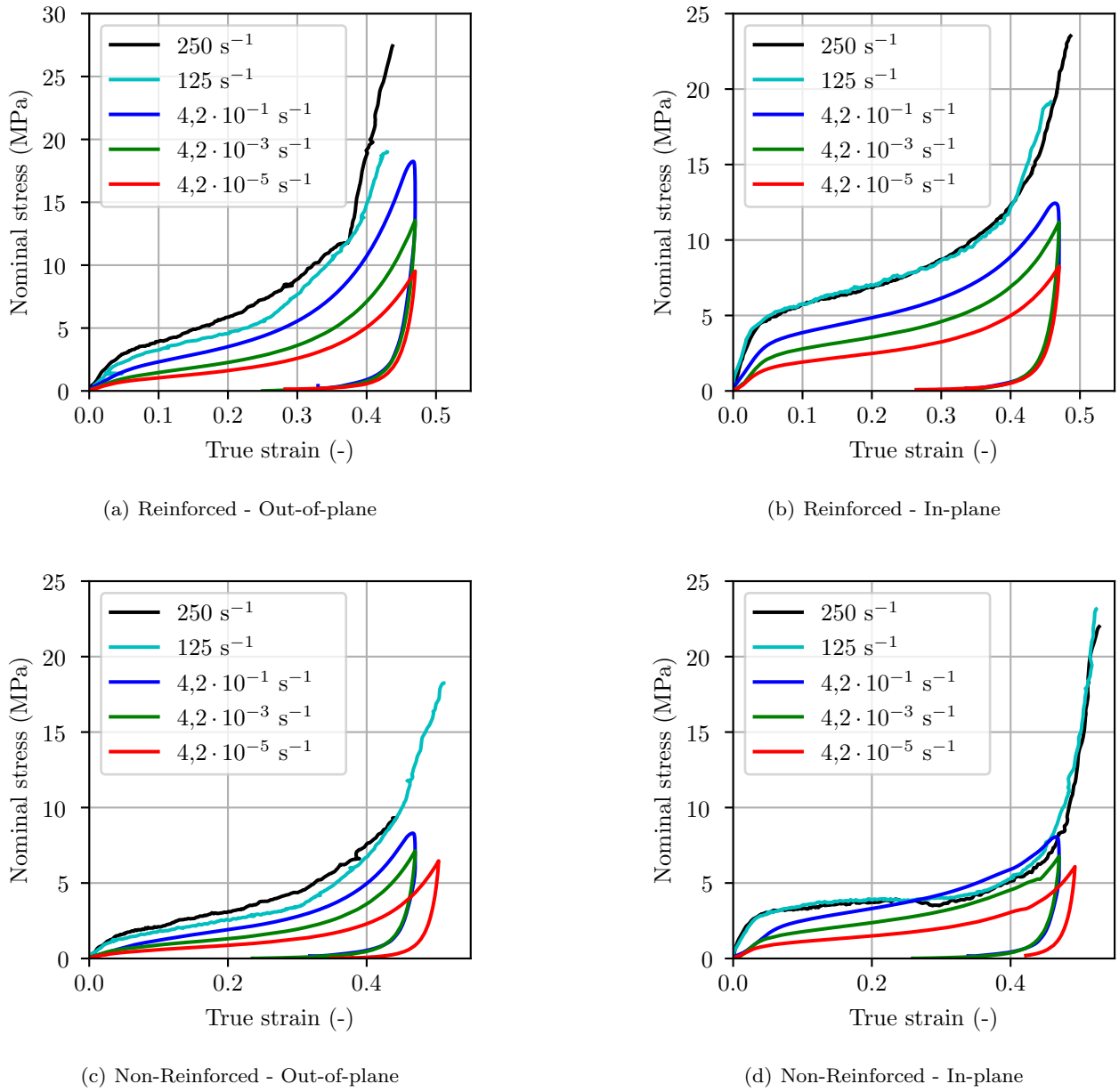

(a) Reinforced - Out-of-plane

(b) Reinforced - In-plane

(c) Non-Reinforced - Out-of-plane

(d) Non-Reinforced - In-plane

Fig. 8 Experimental stress/strain curves of cork agglomerates compressed in the in-plane (IP) and out-of-plane (OP) directions at different strain rates at room temperature (24°C).

Material	ε^*_{frac} à 4,2 10^{-5} s^{-1}	ε^*_{frac} à 4,2 10^{-3} s^{-1}	ε^*_{frac} à 4,2 10^{-1} s^{-1}	ε^*_{frac} à 125 s^{-1}	ε^*_{frac} à 250 s^{-1}
R-OP	X	X	X	X	X
NR-OP	X	X	X	$0.48^{\pm 0.02}$	X
R-IP	X	X	X	$0.41^{\pm 0.03}$	$0.36^{\pm 0.02}$
NR-IP	$0.42^{\pm 0.03}$	$0.42^{\pm 0.05}$	$0.40^{\pm 0.05}$	$0.30^{\pm 0.01}$	$0.28^{\pm 0.02}$

Table 2 Macroscopic strain at which cracks are observed on the surface of the specimens as a function of the average strain rate. IP : In-plane direction. OP : Out-of-plane direction. R : Reinforced cork agglomerate. NR : Non-reinforced cork agglomerate. X : no cracking was observed macroscopically.

3.2.1 Macroscopic curves

Fig. 8 shows the stress/strain curves obtained from compression tests on agglomerated cork specimens at room temperature (24°C) carried out at different strain rates. The bigger the strain rate, the bigger stresses reached during the compression as already reported [11].

In quasi-static regime (at 4.2 10^{-5}; 4.2 10^{-3} and 4.2 10^{-1} s^{-1}), the strain rate varies each time by two decades and a clear difference is observed between each curve for all directions of compression (IP) and (OP) (Fig. 8).

In dynamic regime (at 125 and 250 s^{-1}), such a similar amplitude in strain rates (of 3 decades) was not possible. The two average strain rates only have a ratio of 2 to each other. In the out-of-plane (OP) direction, for both types of agglomerate, there is a difference between the two curves in the dynamic regime (Fig. 8(a) and Fig. 8(c)). On the contrary, in the in-plane direction, the curves at 125 and 250 s^{-1} are close (Fig. 8(b) and Fig. 8(d)).

3.2.2 Fracture mechanisms

As for macroscopic behavior, strain rate has an opposite effect to temperature on the failure initiation and propagation. Cracks appear earlier at the sample surface for tests at high strain rates (tab. 2).

Crack propagation is observed for all compression tests in the in-plane direction of non reinforced cork samples (NR-IP) (tab. 2). For loading at 125 and 250 s^{-1}, the nominal stress after ε_{frac} is lower than the stress for other strain rates (Fig. 8(d)).

The two agglomerates compressed in the in-plane direction show very large barreling at ε^*=0.35 for the agglomerate without fibres (Fig. 9d) and at ε^*=0.45 for the agglomerate with fibres (Fig. 9c). Attempts have been made to reduce the barreling effect by lubricating the plates or by modifying the shape of the specimens. However neither PTFE, grease nor the cylinder shape were able to adresse it. It seems that the high Poisson coefficient in this loading direction [33] coupled with the high friction coefficient of cork [34] lead to a barreling that is difficult to supress. The calculation of the nominal stress therefore no longer seems relevant here and the real cross-section of the specimen would have to be taken into account for further quantitative estimation.

Furthermore, at 250 s^{-1}, fracture mechanisms cause a fragmentation of the sample (Fig. 9d). At this macroscopic strain rate, from ε^*=0.35, the real cross-section S of the specimen decreases abruptly, so the true stress should also increase. Once again, structural effects prevent an in-depth characterisation of the material. Material parameter that will be given in the next section have thus to be taken with caution.

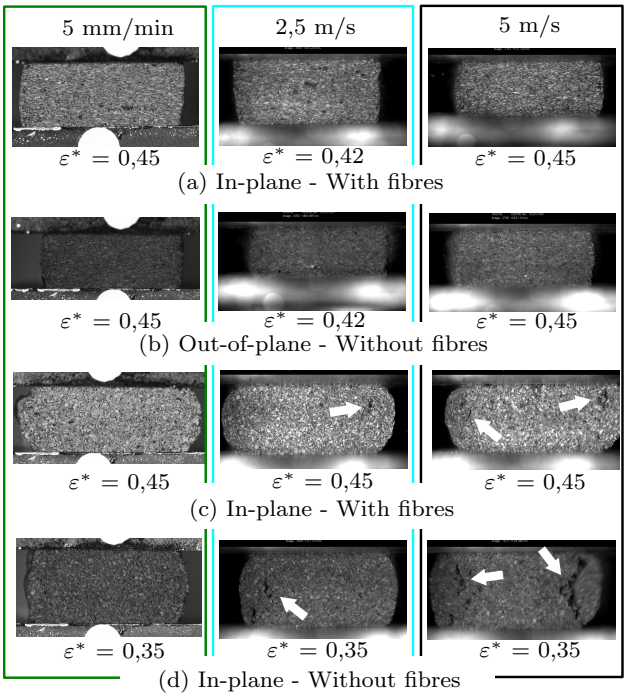

Fig. 9 Picture of the surface of agglomerate specimens tested at room temperature at several strain rates at a given mean strain ε^* if cracks are observed (indicated by white arrows) or at the end of the loading phase if no cracks are observed.

3.2.3 Material parameters

From the stress/strain curves, the variation of the material parameters (Young's modulus E^*, buckling stress σ^*_{fl}, tangent modulus E^*_p and strain at densification ε^*_d) were plotted as a function of the average strain rate for the different cork agglomerates (Fig. 10).

The Young's modulus E^* (Fig. 10(a)) and the tangent modulus E^*_p (Fig. 10(c)) both evolve in a similar non-linear manner with the macroscopic strain rate. They increase relatively slowly over several decades in quasi-static regime. For strain rates belonging to the dynamic regime, above 10^{-1} s^{-1}, the values of these two parameters increase more rapidly.

The macroscopic elastic buckling stress σ^*_{fl} (Fig. 10(b)) also increases with the strain rate. The variation of this parameter is quasi-linear with the logarithm of the macroscopic strain rate, compared to both moduli.

This trend for buckling stress is similar to what has already been observed for strain rates above 0.01 s^{-1} on polymer foams (PVC [35], EPS or natural cellular materials such as balsa [36] or birch plywood [32]). Cork agglomerates and multi-scale expanded polystyrene foams [35] are made of polymers with different visco-elastic be-

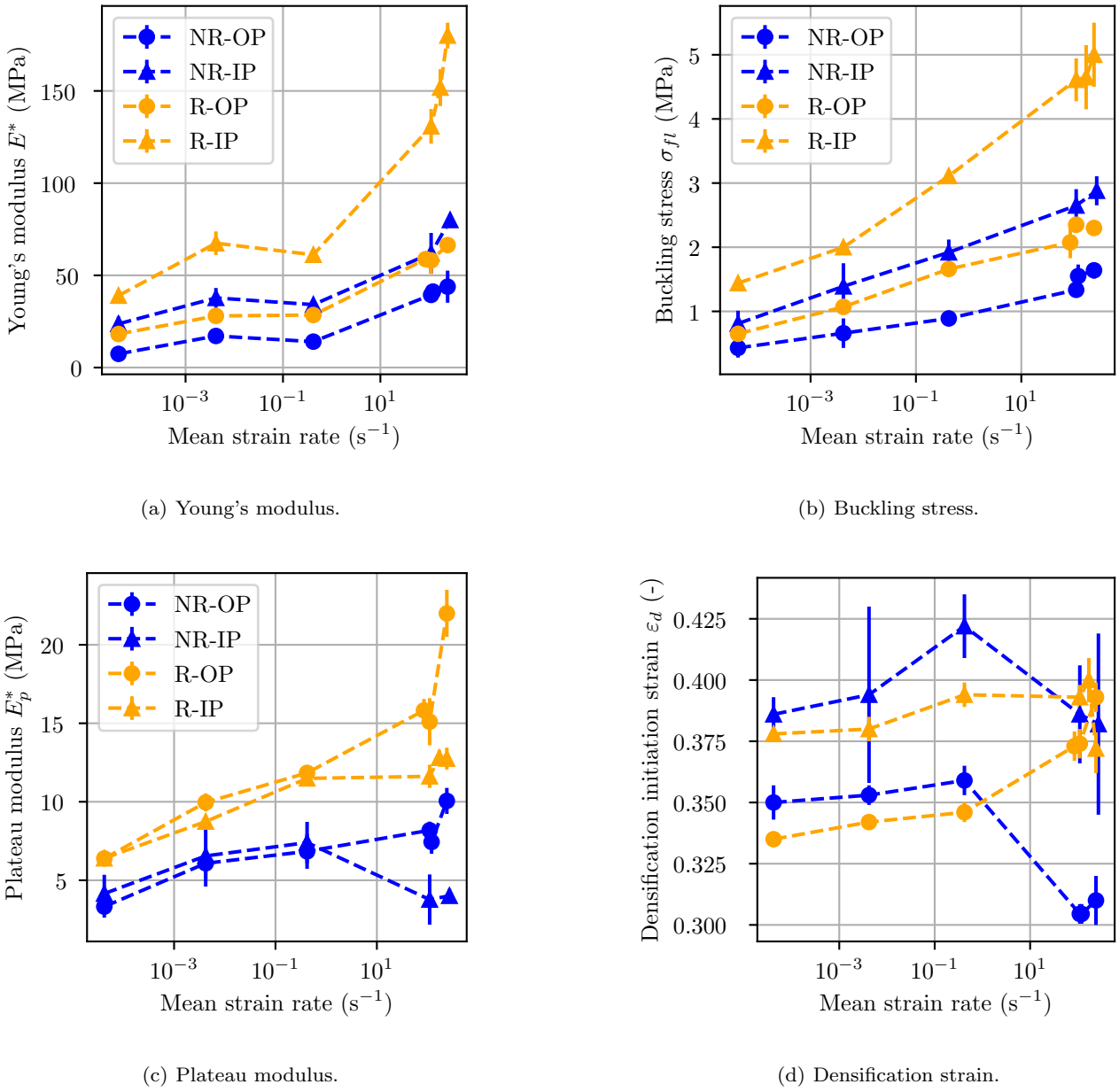

(a) Young's modulus.

(b) Buckling stress.

(c) Plateau modulus.

(d) Densification strain.

Fig. 10 Material parameters of different cork agglomerates compressed at 24°C at several strain-rates.

havior. And yet they show similar trends in the variation of certain macroscopic material parameters. These experimental results could therefore indicate that the dependence on the strain rate of the buckling stress may not simply be due to the inherent dependence of the constitutive materials. Some structural effects could arise as the strain rate increases and reaches dynamic values.

The strain at the initiation of densification ε_d^* increases slightly with the strain rate for reinforced samples (Fig. 10(d)). For non-reinforced samples, ε_d^* slowly increases for strain rates until 10 s^{-1} and then decreases abruptly for dynamic strain rates. This decrease for non-reinforced cork agglomerates could come from the embrittlement of the material with the increase of the strain rate.

For each material, the range of variation of the strain at the onset of the densification has been reported in tab.3.

For plywood birch, the densification strain value remained in the range [0.365, 0.381] [32]. The evolution of the densification strain was only significant for a jump in strain rate by 10^5 s^{-1} with a jump in densification strain value about two time the standard deviation. The

Material	Range
R-OP	[0.335,0.390]
R-IP	[0.378,0.400]
NR-OP	[0.305,0.360]
NR-IP	[0.380,0.420]

Table 3 Range of densification strain for several cork agglomerates.

densification strain increased from 0.365 at 4 10^{-4} s^{-1} to 0.381 at 700 s^{-1}. Cork agglomerates show a wider range of variation, especially for reinforced cork agglomerates loaded in the out-of-plane direction (tab.3). For the reinforced agglomerate, it increases from 0.335 in quasi-static to 0.39 in dynamic, with a rather small standard deviation (Fig. 10(d)).

While the strain at the onset of densification ε_d^* was mostly constant with temperature, it seems that ε_d^* increases slowly with the strain rate as long as the material stays non-brittle. This observation seems to concern several polymeric foam but not in the same extent.

The variation of the material parameters with the strain rate is therefore not the same for all parameters, unlike what has been observed with the variation of the mechanical behavior with temperature.

3.2.4 Absorbed energy evolution with the strain-rate

Absorbed energy before the initiation of the densification W_{abs}^* increases with the mean strain rate (Fig.11). However the trend depends on the material. In contrast to the temperature dependence, the evolution of the absorbed energy is not similar to the other material parameters.

For non-reinforced agglomerated cork, absorbed energy seems to reach a plateau near 10^{-1} s^{-1} (Fig.11). The value of this asymptotic evolution stands around 1 $J\ mm^{-3}$ in the out-of-plane direction and is close to 1.75 $J\ mm^{-3}$ in the in-plane direction. For reinforced cork agglomerates, absorbed energy evolves almost linearly with the mean strain rate logarithm. For the highest strain rates, the absorbed energy strongly increases. These differences in behaviour between reinforced and unreinforced cork could be due to the more brittle nature of the unreinforced material [14].

The evolution of the absorbed energy is stronger between -25°C and 75°C than between 4.2 10^{-5} and 250 s^{-1} for the non-reinforced samples (Fig.11). On the contrary, the absorbed energy values swept over these temperature and strain rate ranges are similar for reinforced samples: between 1.2 and 4 $J\ mm^{-3}$ in the in-plane direction. This supports the hypothesis that for non-reinforced cork agglomerates, high strain rates at

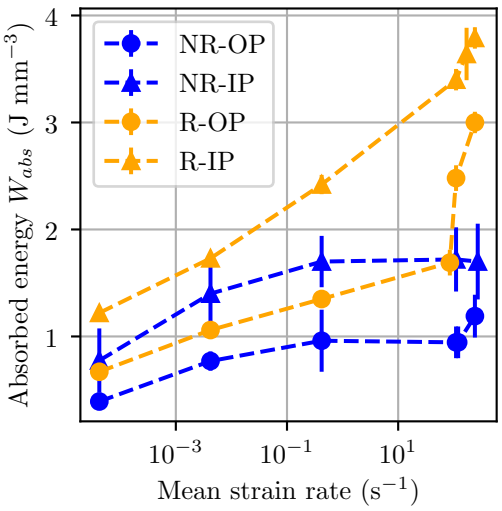

Fig. 11 Absorbed energy at the initiation of the densification for different types of agglomerated cork under several strain-rate conditions.

room temperature undermine the mechanical behaviour of the material.

Like before, the standard deviation σ_{SD} remains relatively small for each materials on the tested strain-rate range (Fig.10 and Fig.11). Only the densification initiation strain ε_d^* of the non-reinforced agglomerate loaded in the in-plane direction shows a great variability at low and high strain rates.

3.2.5 Discussion on strain-rate dependency

The different variation with the strain rate of Young's modulus, buckling stress, tangent modulus and absorbed energy could indicate that the strain rate dependency of the mechanical behavior of cellular materials is not simply due to the visco-elastic behavior of the constitutive materials.

For high-strain rate loadings, special features of cellular solids influence the overall force-displacement response [27]. Inertial energy contained in the rotations and asymmetric deflections associated with buckling modes of deformation can cause inertia at the microscopic scale, *i.e.* a delay in the buckling of cell wall. This delay leads to a deformation mode which can resist higher loads [37].

Moreover when a closed-cell foam, like cork, is compressed, the fluid within the cells is under pressure [18]. For elastomeric foam, the effect of the gas on the plateau phase of the stress-strain curve is very pronounced [38], even for reasonnable ranges of strain rates (between 2×10^{-3} s^{-1} to 50 s^{-1}). For increasing strain rates, gas compression would thus cause an increase in stress.

In order to experimentaly separate such effects, the constitutive material behavior has to be controled. This behavior depends on both temperature and strain rate conditions [39]. That is why a specific experimental set-up was designed in order to operate dynamic compressive tests at controled temperatures. In the next section, the design of the specific apparatus and experimental data obtained are presented and discussed.

3.3 Coupled effect of temperature and strain-rate

3.3.1 Compression apparatus for intermediate strain rate in temperature

The assumption of a constant temperature during intermediate speed compression tests is difficult to make. In order to perform tests at dynamic regime in temperature, a thermal chamber for the fly wheel apparatus was thus designed and build (Fig.12a). The reduced available space around the loading area principally dictated design choices along with the requirement to be able to observe sample deformation (Fig.12b). It is interesting to note that cork was chosen to be the main material of the structure of the thermal chamber (for its good insulation properties [1]).

The inner of the thermal chamber can be conditionned at a desired temperature T_i thanks to an air circuit with a temperature controled using an Arduino micro-controler (Fig.12c and Fig.12d). The two temperature sensors, placed on either side of the thermal chamber, measure respectively T_a and T_b. The temperature of the thermal chamber $T_{chamber}$ is then calculated from these measurements,

$$T_{chamber} = \frac{T_a + T_b}{2}. \tag{6}$$

If $T_{chamber} < T_i$, the resistor is activated. The air in the mixing box is heated and injected into the thermal chamber through insulating sleeves thanks to fans until $T_{chamber}$ is reached. If $T_{chamber} > T_i$, nitrogen is injected inside the mixing box in order to cool down the temperature of the air flow.

In order for the thermal chamber and the metallic punches to reach T_i, 1 to 2 hours are needed. The temperature of the chamber and of the metallic punches is also checked with an infrared thermometer to collect more local data. In the mean time, samples are conditioned in temperature in the same chamber that was used for quasi-static tests. The specimen is placed in the chamber just before the mechanical test. One to two minutes are required to focus the high speed camera placed in front of the set up to observe the deformation of the cubic samples (Fig.12c) and to check the temperature at the sample surface thanks to an infrared thermometer. It takes then around 30 seconds for the fly wheel to reach the wanted rotation speed. Lights are turned on just before the test is carried on. Like previously, the force and the lower punch displacement are then recorded.

Previous results showed that catastrophic failure were more likely to happen for cold or dynamic loadings. Early fracture can imply a lower absorbed energy as for non-reinfroced cork agglomerates. Compression loadings in dynamic regime (63 and 187 s^{-1}) at -20°C were thus operated to test this set-up and to verify if low temperature and high strain-rate induced a significant decrease in the absorption capacity of agglomerated cork.

3.3.2 Macroscopic response and identification of the material parameters

The two compression tests achieved in dynamic regime (63 and 187 s^{-1}) at -20°C were compared to previous compression tests realised either in dynamic regime (187 s^{-1}) at room temperature or in quasi-static regime at $-$ 30°C (Fig. 13).

In dynamic regime and at low temperatures, the stresses reached by the different agglomerates are more important, except for NR-IP samples, than for loadings at either low temperature or high strain-rate (Fig. 13). This shows,as expected, that the combination of strain rates and temperature is important to take into account when studying the mechanical behavior of such materials.

The material parameters of the two compression tests carried out in dynamic regime (63 and 187 s^{-1}) at -20°C were then compared to those obtained in quasi-static regime at room temperature (tab.4). The material parameters, such as Young's modulus E^*, buckling stress σ^*_{fl} or energy absorbed W^*_{abs} before densification, measured from these curves are much more important in these severe conditions than those measured in quasi-static regime (tab. 4). The increase in strain rate and the decrease in temperature mainly modify Young's modulus E^* and buckling stress σ^*_{fl}. These parameters for all types of cork agglomerates increase by more than 150 % under these severe conditions (tab. 4). However, the Young's modulus values indicate that the glass plateau is not reached yet for the constitutive materials (tab. 4). Indeed, DMA tests showed values for the storage modulus E' up to 300 MPa (IP-R) and 150 MPa (OP-R) [14], while they only reached here 192 MPa and 118 MPa, respectively. Strain rates up to 187 s^{-1} in combination with a temperature of -20°C

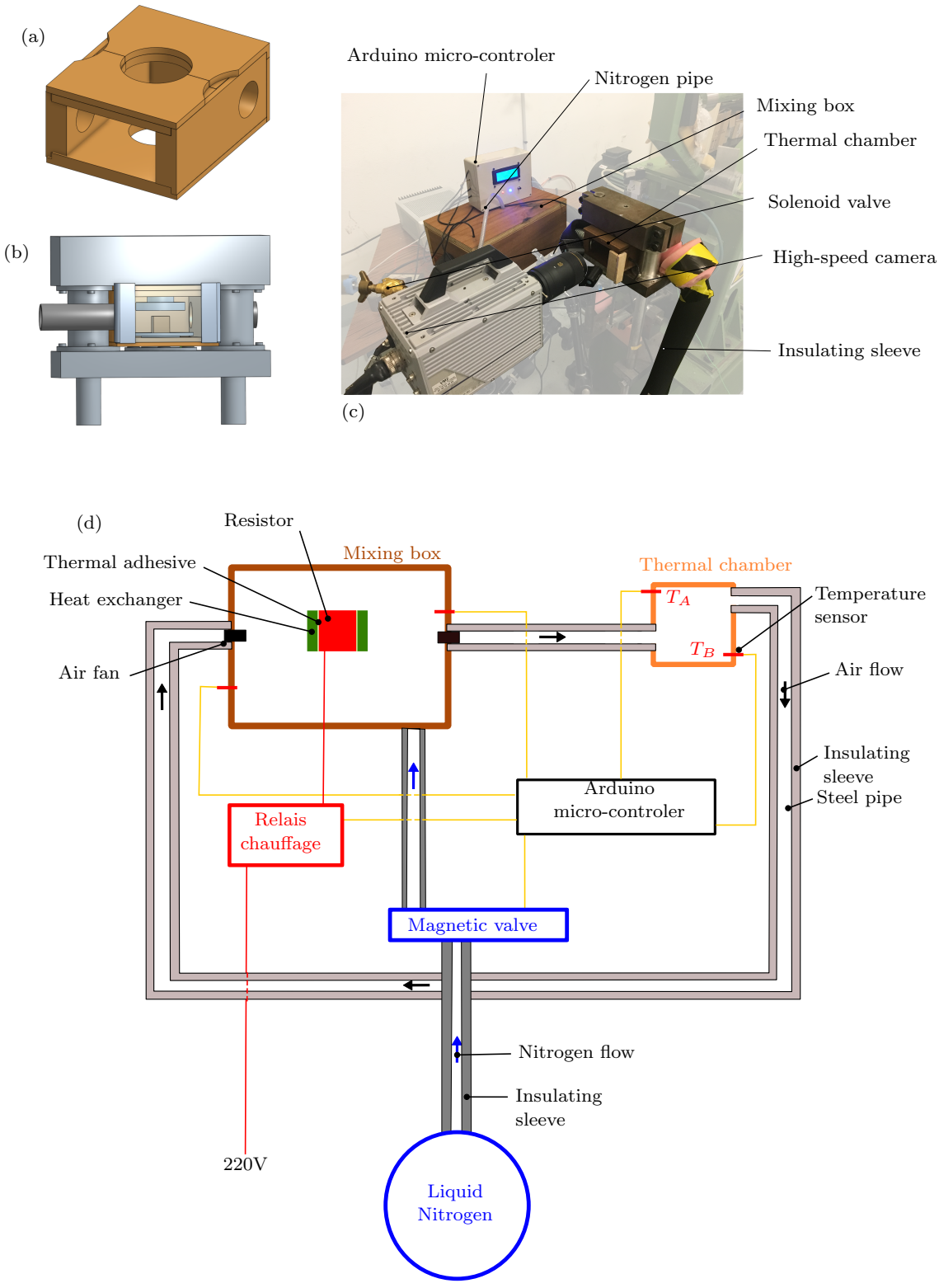

Fig. 12 (a) Thermal set-up with the CAD of the thermal chamber. (b) CAD of thermal chamber placed in the loading area. (c) Experimental set-up of controlled temperature compression tests at intermediate strain rates. (d) Scheme of the temperature set-up.

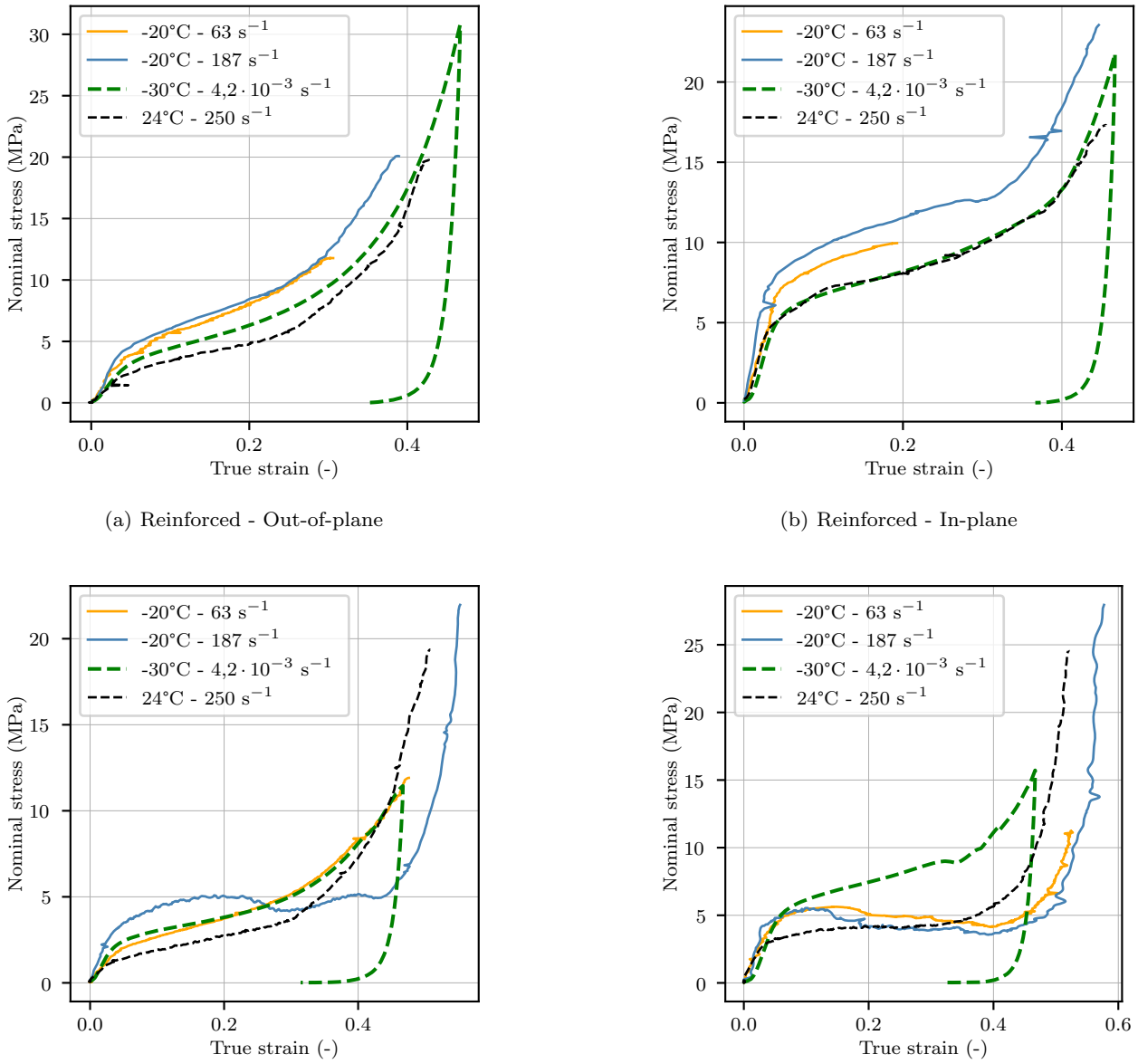

(a) Reinforced - Out-of-plane

(b) Reinforced - In-plane

(c) Non-reinforced - Out-of-plane

(d) Non-reinforced - In-plane

Fig. 13 Experimental stress/strain curves of cork agglomerate samples loaded at -20°C in dynamic regime compared to data obtained either in quasi-staitc at -30°C or at 24°C in dynamic regime.

are therefore not sufficient to reach the glass plateau of the constitutive materials for agglomerates.

For cork agglomerates with fibres (R), the increase in the strain rate associated with a decrease in temperature has a non-negligible effect on the decrease of the densification strain ε_d^* (tab. 4). This parameter varied only slightly with simply temperature or average strain rate during previous stresses, whereas it decreases by 34 and 28% respectively under out-of-plane (R-OP) and in-plane (R-IP) compression when the effects of strain rate and temperature are cumulated. This effect is much less highlighted for non-reinforced agglomerates (NR), as the densification strain ε_d^* decreases by only 1 % under a out-of-plane (NR-OP) compression and 15% under an in-plane (NR-IP) compression (tab. 4). The interaction of different deformation mechanisms (fracture for NR samples) in the plateau phase could be the cause of these two different behaviors.

Material	E* [MPa]	σ^*_{fl} [MPa]	E^*_p [MPa]	ε^*_d [-]	W^*_{abs} [J/mm^3]
NR-OP	22,00 ± 1,0	0,83 ± 0,06	5,77 ± 0,42	0,455 ± 0,008	0,93 ± 0,08
-20°C, 187 s^{-1}	87	3,5	2,92	0,45	2,52
	+ 295%	+ 322 %	- 49 %	- 1 %	+ 171 %
R-OP	27,7 ± 1,9	1,08 ± 0,04	8,39 ± 0,34	0,457 ± 0,002	1,32 ± 0,06
-20°C, 187 s^{-1}	118	4,2	22,1	0,3	2,49
	+ 326 %	+ 289 %	+ 163 %	- 34 %	+ 89 %
NR-IP	36,0 ± 2,9	1,2 ± 0,13	4,47 ± 0,57	0,530 ± 0,005	1,28 ± 0,06
-20°C, 187 s^{-1}	93	4,4	-9,9	0,426	2,09
	+ 158 %	+ 267 %	- 321 %	- 15 %	+ 63 %
R-IP	61,2 ± 4,5	2,07 ± 0,04	7,04 ± 0,11	0,501 ± 0,005	1,99 ± 0,04
-20°C, 187 s^{-1}	192	5,7	15,5	0,362	4,4
	+ 214 %	+ 175 %	+ 120 %	- 28 %	+ 121 %

Table 4 Material parameters of agglomerated cork (NR) and short fibre reinforced agglomerated cork (R) tested in compression in the out-of-plane (OP) and in-plane (IP) directions at either a macroscopic strain rate of 4.2 10^{-3} s^{-1} at room temperature (24°C) or a macroscopic strain rate of 187 s^{-1} at -20°C

3.3.3 Modification of the fracture mechanisms

Non-reinforced (NR) cork agglomerates have a plateau phase under severe loading that is different from previous results. The modulus E^*_p decreases in the out-of-plane direction (NR-OP) and becomes negative for in-plane compression (NR-IP) (tab. 4). This change in the plateau phase under severe loading (Fig. 13) is mainly due to the earlier appearance of failure mechanisms under these conditions (Fig. 14c and Fig. 14d).

In the case of NR-OP samples, the mechanical behavior is strongly modified at -20°C between 63 s^{-1} and 187 s^{-1} (Fig. 13c). Photographs of the specimens surface taken during the test also shows a change in fracture mechanisms. At 63 s^{-1}, cracks are only visible from ε^*=0.4 (Fig. 14c). These are located at the periphery of the specimen, as described above for specimens compressed in the in-plane direction. Photographs of specimens compressed at 187 s^{-1} at -20°C show that many cracks appear at the centre of the specimen at a macroscopic strain much lower than ε^*=0.24 (Fig. 14c). Same observations are made for NR-IP sample around ε^*=0.08.

3.3.4 Absorbed energy

In comparison to the results obtained in quasi-static regime at room temperature, cork agglomerates absorb more energy at low temperature and high strain-rate (tab. 4). This remarks could have been done from the tendencies observed either at several temperatures or different strain-rates. However, values of absorbed energy are lower than expectations. Precedent values at -20°C or in dynamic regime (Fig. 7 and Fig. 11) were around the same order of magnitude than for -20°C and dynamic tests.

Observations have shown that fracture mechanisms appear very prematurely under these conditions. Cracks can be observed on the surface from ε^*=0.08, *i.e.* from the beginning of the plateau phase (Fig.14). The appearance of these cracks is different from what has been observed for less severe conditions (lower strain rates or higher temperature). At lower strain rates or higher temperatures, the cracks appeared at the periphery of the specimen, due to barreling. For agglomerates under dynamic loadings at -20°C, cracks now appear in the diagonal of the specimen (Fig. 14c and Fig. 14d).

In conclusion, the strain mechanisms involved in the plateau phase, which allow to absorb the mechanical energy, are therefore not the same between compression tests under one environnemental condition that is severe that under a combination of severe conditions (temperature and strain-rate).

4 Conclusions & Perspectives

The aim of this work was to study the mechanical behavior of a natural polymeric foam, cork agglomerate, and its dependencies to temperature and strain rate during a compressive loading.

Temperature and strain rate are two environnemental conditions intrinsically linked for small strains. It was indeed observed that either for increasing temperature and decreasing strain-rate, a drop of the stress could be observed on the macroscopic behavior. A non-linear dependency was observed in the initial rigidity for both temperature and strain-rate. The same variation was noticed in temperature for several material parameters reflecting very different stages in the compression loading (Young's modulus, plateau modulus, buckling stress and absorbed energy). This temperature dependency was associated to the visco-elastic behavior of cork, one of the constitutive materials. It is interesting to note that this visco-elastic behavior is also ex-

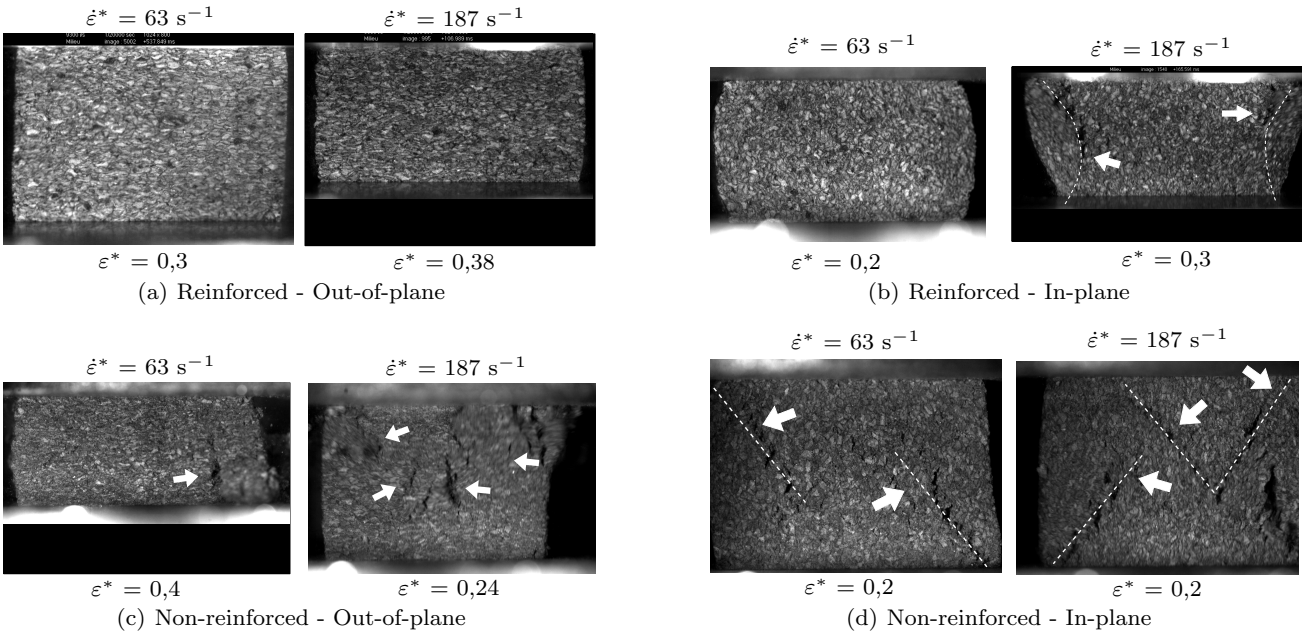

(a) Reinforced - Out-of-plane (b) Reinforced - In-plane

(c) Non-reinforced - Out-of-plane (d) Non-reinforced - In-plane

Fig. 14 Pictures of the surface of agglomerated cork specimens with and without fibres, loaded at -20°C in dynamic regime. The white arrows indicate the presence of cracks and the dotted lines show the crack pattern on the surface of the specimens.

pressend on the non-linear beahvior of the composite material (plateau phase).

The variation of material parameters with strain rate was less trivial. Because of the non-linear mechanisms involved during a compression loading in such materials, the hypothesis of *structural effect* modifying the mechanical behavior may be considered.

A first attempt to distinguish the constitutive material dependency from the structural effect was made by conducting mechanical tests at chosen strain rates and temperatures. For that, a specific experimental set-up was developed in order to operate mechanical tests in temperature at high strain rate on a fly wheel. The proof-of-concept was done by conducting tests at -20°C in dynamic regime. The results showed new fracture mechanisms under these severe loadings.

Perspectives of this work would be to develop a model taking into account the visco-elastic behavior of the constitutive material to predict the non-linear macroscopic behavior of cellular material and its dependency to temperature and strain rate. A more fondamental perspective would also to separate more closely what causes the strain-rate/temperature dependency between material and structure dependencies by using the set-up developped in this work.

Acknowledgements This work was performed in the framework of the LIAMA project (supported by Lieges HPK, Safran Power Unit (PU) and Région Nouvelle Aquitaine). The authors are very grateful to Agnès de Montbrun and Olivier Pauly from Lieges HPK and Romain Quinton from Safran PU for their scientific and technical contributions to this study. Thanks to Valentin Honno for his help during the conception of the thermal chamber.

Conflict of interest

The authors declare that they have no conflict of interest.

References

1. L.J. Gibson, K.E. Easterling, M.F. Ashby, Proceedings of the Royal Society A: Mathematical, Physical and Engineering Sciences **377**(1769), 99 (1981). DOI 10.1098/rspa.1981.0117
2. M.E. Rosa, M. Fortes, Mater. Sci. Eng. A 111 **100**, 217 (1988)
3. A. Sen, J. Van Den Bulcke, N. Defoirdt, J. Van Acker, H. Pereira, Thermochimica Acta **582**, 94 (2014). DOI 10.1016/j.tca.2014.03.007
4. A. Lagorce-Tachon, T. Karbowiak, D. Champion, R.D. Gougeon, J.P. Bellat, Materials and Design **82**, 148 (2015). DOI 10.1016/j.matdes.2015.05.034
5. F.A.O. Fernandes, R.J.S. Pascoal, R.J. de Sousa, Materials Design **58**, 499 (2014). DOI 10.1016/j.matdes.2014.02.011
6. S. Sanchez-Saez, S.K. García-Castillo, E. Barbero, J. Cirne, Materials Design **65**, 743 (2015). DOI 10.1016/j.matdes.2014.09.054
7. P.T. Santos, S. Pinto, P.A. Marques, A.B. Pereira, R.J. Alves de Sousa, Composite Structures **178**, 277 (2017). DOI 10.1016/j.compstruct.2017.07.035. URL http://dx.doi.org/10.1016/j.compstruct.2017.07.035

8. M. Ptak, P. Kaczyński, J. Wilhelm, J.M. Margarido, P.A. Marques, S.C. Pinto, R.J. de Sousa, F.A. Fernandes, Materials **12**(1) (2019). DOI 10.3390/ma12010151
9. M. Sasso, E. Mancini, G. Chiappini, F. Sarasini, J. Tirillò. Application of DIC to Static and Dynamic Testing of Agglomerated Cork Material (2018). DOI 10.1007/s11340-017-0369-9
10. C.P. Gameiro, J. Cirne, International Journal of Mechanical Sciences **49**(9), 1029 (2007). DOI 10.1016/j.ijmecsci.2007.01.004
11. C.P. Gameiro, J. Cirne, G. Gary, Journal of Materials Science **42**(12), 4316 (2007). DOI 10.1007/s10853-006-0675-6. URL http://link.springer.com/10.1007/s10853-006-0675-6
12. M. Ptak, P. Kaczynski, F.A. Fernandes, R.J. de Sousa, International Journal of Impact Engineering **106**, 238 (2017). DOI 10.1016/j.ijimpeng.2017.04.014
13. P. Kaczynski, M. Ptak, J. Wilhelm, F.A. Fernandes, R.J. de Sousa, International Journal of Impact Engineering **126**(November 2018), 109 (2019). DOI 10.1016/j.ijimpeng.2018.12.001. URL https://doi.org/10.1016/j.ijimpeng.2018.12.001
14. L. Le Barbenchon, J.B. Kopp, J. Girardot, P. Viot, Mechanics of Materials (2020)
15. L. Le Barbenchon, J. Girardot, J.B. Kopp, P. Viot, Materialia **5** (2019). DOI 10.1016/j.mtla.2019.100219
16. P. Viot, International Journal of Impact Engineering **36**(7), 975 (2009). DOI 10.1016/j.ijimpeng.2008.11.010
17. P. Viot, International Journal of Impact Engineering **36**(7), 975 (2009). DOI 10.1016/j.ijimpeng.2008.11.010
18. R. Bouix, P. Viot, J.L. Lataillade, International Journal of Impact Engineering **36**(2), 329 (2009). DOI 10.1016/j.ijimpeng.2007.11.007
19. M. Avalle, G. Belingardi, R. Montanini, International Journal of Impact Engineering (2001). DOI 10.1016/S0734-743X(00)00060-9
20. Q.M. Li, I. Magkiriadis, J.J. Harrigan, Journal of Cellular Plastics **42**(5), 371 (2006). DOI 10.1177/0021955X06063519
21. T. Thomas, H. Mahfuz, L.A. Carlsson, K. Kanny, S. Jeelani, Composite Structures **58**(4), 505 (2002). DOI 10.1016/S0263-8223(02)00159-9
22. B. Song, W.Y. Lu, C.J. Syn, W. Chen, Journal of Materials Science **44**(2), 351 (2009). DOI 10.1007/s10853-008-3105-0
23. H. Pereira, Wood Science and Technology **22**(3), 211 (1988). DOI 10.1007/BF00386015
24. S.P. Silva, M.A. Sabino, E.M. Fernandes, V.M. Correlo, L.F. Boesel, R.L. Reis, International Materials Reviews **50**(6), 345 (2005). DOI 10.1179/174328005X41168
25. A. Lagorce-Tachon, T. Karbowiak, D. Champion, R.D. Gougeon, J.P.P. Bellat, Journal of Materials Science **51**(9), 4227 (2016). DOI 10.1007/s10853-015-9669-6. URL http://link.springer.com/10.1007/s10853-015-9669-6
26. C. Menager, N. Guigo, X. Wu, L. Vincent, N. Sbirrazzuoli, Composites Part A: Applied Science and Manufacturing **124**(February), 105473 (2019). DOI 10.1016/j.compositesa.2019.105473. URL https://doi.org/10.1016/j.compositesa.2019.105473
27. L.J. Gibson, M.F. Ashby, *Cellular Solids: Structure and Properties*, cambridge edn. (Cambridge University Press, Oxford, 1997)
28. Y. Sun, Q.M. Li, International Journal of Solids and Structures **63**, 50 (2015). DOI 10.1016/j.ijsolstr.2015.02.034
29. J.A. Elliott, A.H. Windle, J.R. Hobdell, G. Eeckhaut, R.J. Oldman, W. Ludwig, E. Boller, P. Cloetens, J. Baruchel, Journal of Materials Science **37**(8), 1547 (2002). DOI 10.1023/A:1014920902712
30. V. Marcadon, Comportement mécanique des architectures cellulaires -Du matériau à la structure-. Habilitation à diriger des recherches, Université Paris-Saclay (2019)
31. K.R. Mangipudi, S.W. Van Buuren, P.R. Onck, International Journal of Solids and Structures **47**(16), 2081 (2010). DOI 10.1016/j.ijsolstr.2010.04.009. URL http://dx.doi.org/10.1016/j.ijsolstr.2010.04.009
32. L. Caetano, V. Grolleau, B. Galpin, A. Penin, J.D. Capdeville, Strain **54**(2) (2018). DOI 10.1111/str.12264. URL https://doi.org/10.1111/str.12264
33. L. Le Barbenchon, Description multi-échelles du comportement mécanique d'un matériau cellulaire composite sous sollicitations sévères. - Application aux agglomérés de liège pour l'aéronautique -. Ph.D. thesis, Arts et Métiers ParisTech (2020)
34. L.J. Gibson, The elastic and plastic behaviour of cellular materials. Ph.D. thesis, University of Cambridge (1981)
35. B. Song, W.W. Chen, S. Dou, N.A. Winfree, J.H. Kang, International Journal of Impact Engineering **31**, 509 (2005). DOI 10.1016/j.ijimpeng.2004.02.003
36. V.L. Tagarielli, V.S. Deshpande, N.A. Fleck, Composites Part B: Engineering **39**, 83 (2008). DOI 10.1016/j.compositesb.2007.02.005
37. Y. Sun, Q.M. Li, International Journal of Impact Engineering **112**(February 2017), 74 (2018). DOI 10.1016/j.ijimpeng.2017.10.006
38. J. Zhang, N. Kikuchi, V. Li, A. Yee, G. Nusholtz, International Journal of Impact Engineering **21**(5), 369 (1998). DOI 10.1016/s0734-743x(97)00087-0
39. J.L. Halary, F. Lauprêtre, *Mécanique des matériaux polymères* (Humensis, 2015)